Electrical Power and Energy Systems 151 (2023) 109198

Contents lists available at ScienceDirect

International Journal of Electrical Power and Energy Systems

journal homepage: www.elsevier.com/locate/ijepes

# Artificial vision wireless PV system to efficiently track the MPP under partial shading

Aranzazu D. Martin [a,*], Juan M. Cano [a], Jonathan Medina-García [b], Juan A. Gómez-Galán [b], Adoración Hermoso [b], Jesus R. Vazquez [a]

[a] Departament of Electrical Engineering, University of Huelva, Huelva 21007, Spain
[b] Departament of Electronic Engineering, Computers, and Automation, University of Huelva, Huelva 21007, Spain

ARTICLE INFO

*Keywords:*
Artificial Vision
IEEE 802.15.4 communication
Partial Shading
PV Monitoring Systems
Wireless Sensor Network

ABSTRACT

The solar photovoltaic industry is booming and the achievement of high efficiency in this kind of systems is crucial. Partial shading conditions complicate the search of the maximum power point (MPP) of the installations due to the existence of multiple peaks in the P-V curve. In addition, these photovoltaic (PV) systems require monitoring and control in real-time to guarantee the correct operation. Thus, this paper proposes a novel system to track the maximum power point through artificial vision, under partial shading conditions controlled and monitored by a wireless sensor network based on IEEE 802.15.4 technology. The infrastructure consists of a wireless distributed photovoltaic system (WDPS) where the power converter is connected to a sensor node that sends the information to the coordinator node. The coordinator node is connected to a webcam and a Raspberry Pi. This part of the system is called wireless webcam centralized control (WWCC) and is responsible for processing the sensors information and the images. Besides, the WWCC sends the control signal. The wireless communication is set in beacon-enabled mode allowing synchronization between the sensor nodes and the coordinator node. Moreover, the guaranteed time slot mechanism provides the correct transmission of data with low latency, ensuring the stability of the controller. Experimental tests have been carried out to validate the artificial vision wireless PV system. The results prove an appropriate operation, achieving an MPP tracking higher than 99%, even in partial shading conditions.

## 1. Main text

It is doubtless that nowadays ~~the~~ photovoltaic energy is a big help in reducing the greenhouse gas emissions in the world, producing clean energy without burdening the environment. The breakthrough of the photovoltaic energy is thanks to both its large-scale use, with huge power plants, and small-scale use, due to the self-consumption [1]. Thus, it is crucial for the photovoltaic systems to be efficient, operating at the MPP to guarantee high efficiency and reduce the losses. In addition, to make these systems more profitable, they should use low-cost technology for both the generation and the control system. Besides, an easy maintenance is also important.

The monitoring of the main operating parameters in conventional PV systems is a critical task for the operation of these power plants. Electrical parameters, such as current and voltage, as well as ambient parameters like the irradiance or temperature are usually monitored, conventionally by means of wired sensor technologies. Their high installation and maintenance costs make these technologies inadequate for the increasing number of renewable energy installations, yet real-time monitoring of these plants is required to minimize the impact of the variable energy source on the electricity generation.

The evolution suffered by the classical PV monitoring and control systems allows for new sensor and actuator technologies to be applied, together with wireless communication protocols for the transmission of both acquired data and control instructions [2]. Wireless sensor networks (WSNs) present themselves as a promising technology for the development of smart remote monitoring systems for renewable energy, providing low-cost and simple deployment, as well as flexibility. As such, the data required to optimize the PV generation by means of predictive algorithms could be transmitted through WSNs [3]. A common requirement in all WSN applications is the need for a large number of nodes that must operate without human intervention for long periods of time, while being battery powered. Thus, the optimal application of WSNs in PV systems is conditioned by their efficiency and reliability,

* Corresponding author.
*E-mail address:* aranzazu.delgado@die.uhu.es (A.D. Martin).

https://doi.org/10.1016/j.ijepes.2023.109198
Received 26 June 2022; Received in revised form 3 March 2023; Accepted 27 April 2023
Available online 7 May 2023

which mainly depend upon their communication performance in terms of packet errors, latency, and security, considering a harsh environment. For these reasons, the performance of communication protocols is important in the context of WSNs applied to smart PV systems.

The application of WSN networks in PV systems is becoming of importance in recent years, but it is a field that is under exploration. There are some studies on wireless technology used in PV systems for the monitoring of the parameters of interests using ZigBee and Bluetooth protocols [4–7]. However, although both wireless technologies provide suitable designs, they lack the capacity to comply with the tight requirements of latency and reliability, and require additional hardware for packaging and transmitting data.

The battery powered nature of WSN nodes increases the importance of energy efficiency in their operation. For this reason, over the past few years the IEEE 802.15.4 standard has gained much interest, since it provides a good solution for long term operation by addressing the energy efficient operation, as well as secure data transmission [8]. Furthermore, by efficiently routing the data through the sensing nodes, the deployment of large-scale networks is supported. Therefore, the IEEE 802.15.4 standard has been chosen for communications because it is a low complexity protocol, which allows the deployment of different network topologies and the data can be transmitted in a way that is periodic, intermittent, or with low reaction time.

The PV systems, which usually consist of PV modules, power converters, and a control system, work by means of a maximum power point tracking (MPPT) algorithm to search the MPP under all circumstances. For that, there are a wide variety of MPPTs. The classical methods encompass perturb and observe (P&O), hill climbing, incremental conductance, and ripple correlation control, amongst others [9–12]. Although the P&O represents the most widely used method, the fast tracking has to be compromised with the steady state fluctuations when defining the proper step size. Generally, these conventional techniques are simple and suitable for tracking the MPP, but they exhibit considerable oscillations in power output and reduced efficiency, and they are limited to uniform solar conditions where the P-V curve presents only one maximum power peak. Other more complex algorithms that provide more robustness, speed and accuracy, such as, sliding mode control or backstepping controllers have been recently reported [13–15].

However, the power output from the solar power system generates multiple peaks under partial shading conditions, including one global MPP and many other local peaks, which complicates the above conventional MPPT techniques when searching for the real maximum [16]. Nevertheless, improvements and expansions of these techniques were able to allow MPP tracking under partial shading conditions [17–20]. However, some of these works do not consider the steady state oscillation and divergence problems.

Other promising methods that deal with partial shading are based on computational methodologies usually labelled as intelligent MPPT techniques. The recent proliferation of these trackers is evident using artificial neural network (ANN), particle swarm optimization (PSO), fuzzy logic (FL), and hybrid methods [21–23].

FL has proven itself as an effective solution without the need for accurate system data. It has been shown to provide higher power efficiency when there is a change in irradiance or load current compared with conventional algorithms [24–26]. The main drawbacks are related to the difficulty in deriving fuzzy rules, the need for time consuming, complex calculations, the inability to automatically learn from the environment, and the need for a huge amount of data while running the fuzzification processes.

ANN operates like a black box model, requiring no detail information about the PV system. The weights of the interconnections among neurons can be determined after a learning process using a training dataset. The advantages of ANN include fast response and tracking speed, small fluctuations in steady state, and no need to be reprogrammed. However, for a proper performance, ANN requires a massive amount of data while training the networks, and the complexity is high, as well as the computation time [27,28]. FL and ANN have relatively poor performance in terms of convergence speed and their ability to track under partial shading conditions.

The most common MPPT based on swarm intelligence is the PSO algorithm. The literature describes three main categories of applying PSO to MPPT: standard PSO, improved PSO, and hybrid PSO. In the standard PSO [29], finding the optimum number of iterations required to obtain the global MPP is a difficult task, often leading to convergence problems and power wasting. The modified PSO, does not require huge amounts of training data and is used when multiple maxima are found in the PV characteristics of an array structure under partial shading conditions [30,31]. In the case of the modified PSO, as well as for PSO algorithms integrating techniques for direct updating such as P&O, the approach that allowed solving the convergence problems was the provision of distinct search spaces for each particle. Nevertheless, this approach results in a sizeable random search that generates oscillations, together with an increased computational load for the processor, given the vast number of particles required in order to completely cover the area.

The term Hybrid MPPT is a generic way to refer to the integration of two or more intelligent or conventional MPPT techniques, and where the hybrid method possesses the best attributes of each of the underlying approaches. In this context, algorithms like ANN, FL, or PSO, are appropriate to be integrated with traditional MPPT techniques, such as P&O, or the incremental conductance method [32–35]. The use of such hybrid techniques has led to a better response to changes in the operating point, resulting in improved performance compared to standard methods. Their drawbacks, however, are the increased level of complexity and subsequent slower response, notably detrimental under rapidly varying levels of irradiance. A number of methods that combine FL-based MPPT with PSO can be found in [36,37].

The method known as adaptive neuro-fuzzy interference system (ANFIS) is another widespread hybrid MPPT, having the advantages of both ANN and FL [38,39]. For this method, the ANN is trained to find the optimal MPP, and its output drives an FL-based MPPT. An advantage of both ANFIS and fuzzy logic is the fact that they are optimal, and their flexibility allows them to be adapted to virtually any configuration to accommodate solar energy systems and intelligent energy management. Fuzzy-logic-based classification is able to integrate even classical machine learning (ML) algorithms. This integration, which makes use of a classification system based on supervised learning, allows to determine the optimal step size for the provided meteorological conditions [40,41]. Altogether, the hybrid MPPT offers a good balance of performance and complexity, combining the best characteristics of conventional and intelligent MPPT algorithms.

The intelligent trackers are normally capable of avoiding the local maxima in cases of partial shading, their fast response doesn't overshoot, and for rapidly changing temperature and irradiance values exhibit fewer oscillations in their steady state, compared to classical MPPT approaches. However, the cost of these improvements is the considerable processing power that is necessary, together with significant computational and storage requirements, making them difficult to implement. A good balance between cost, or complexity, and performance, is crucial when applying MPPT to a particular field.

There are also new methods and emerging algorithms, such as, artificial bee colony [42], the Sudoku reconfiguration [43], Kalman filter [44], or Lambert W function [45], amongst others [46,47]. There are also other methods for grid-integrated solar PV systems that are able to attenuate the harmonic components, noise, and DC offset, providing power factor correction or harmonic elimination, and improving the power quality of the system. These techniques are the power normalized kernel least mean fourth algorithm based neural network (NN) control (PNKLMF-NN) technique and learning-based hill climbing (L-HC) MPPT algorithm [48], the gradient descent least squares regression (GDLSR)-based neural network (NN) structure [49], the steepest descent Laplacian regression (SDLR) based adaptive control technique [50], and the

enhanced second order generalized integrator (ESOGI) [51]. In addition, there is another algorithm, which uses a battery for accurate harmonics to supply the load when it is required, or to operate as a distribution static compensator to supply reactive power, the ANOVA Kernel Kalman Filter (AKKF)-based adaptive control algorithm [52].

Regarding the implementation complexity and cost, some key benefits of simple and conventional MPPT algorithms are their low power consumption, reduced likelihood of failure, and lower costs. Their hardware implementation can be achieved with either analog or digital circuitry, as well as a software-based approach using a microprocessor. The flexibility for intelligent MPPTs is lower, since the calculation they require usually confine them to the digital approach. Nevertheless, there are a variety of processor that are suitable for implementing MPPT algorithms, such as the TMS series DSP processors from Texas Instruments, microcontrollers from the PIC/dsPIC series from Microchip, the controllers from dSPACE, or FPGAs, to name a few. The choice for a given type of processor is conditioned by the computational complexity of the MPPT algorithm to be implemented. As a consequence, while the system costs can be brought down by making use of low-cost processors, this option is only applicable to algorithms with low computational requirements, thus excluding methods like ANN, FLC, or the sliding mode controller, for example. With a high-performance processor, there are notable improvements in terms of accuracy and communication speed, but its higher price can impact the system cost. Therefore, the choice for a given processor has to be made considering a trade-off between required performance and acceptable costs for the system.

In this work, an MPPT algorithm under partial shading conditions is designed using artificial vision by means of a low-cost camera. This method detects the non-uniform shading conditions in real time and ~~it~~ is able to search for the MPP and reach it with high efficiency. A customized wireless sensor network solution based on the IEEE 802.15.4 standard has been developed to ensure the stable performance of the control system. This standard in beacon-enabled mode allows for synchronization between the different wireless nodes of the system, and the configuration of the GTS (guaranteed time slot) mechanism enables the data monitoring with a fixed latency.

## 2. Wireless artificial vision PV system architecture

A WSN can be deployed over a whole PV system, making it suitable as a reliable and intelligent solution. However, its correct operation is dependent upon communication technologies that have to assure the transmission of measured sensor data and actuator commands.

There are cases in which a WSN operates in a specific, well-defined scenario, which requires for an existent protocol to be adapted to the particularities of the WSN to optimize communication performance, and also to maximize sensor node battery life. As a consequence, there has been an evolution in the medium access control (MAC) protocols to match the specific needs of WSNs, with new routing algorithms designed to reduce energy consumption. In the IEEE 802.15.4 standard, core requirements such as low-cost, low complexity and very low power consumption are considered. The physical and MAC layers that it defines are specified for low-data-rate wireless connectivity. The physical layer defines the radio bands to be used, as well as the type of spreading and modulation techniques, and is responsible for the data transmission and reception. The MAC layer manages the access to channel, beacon transmission, as well as network association and disassociation. This layer is located just above the physical layer. The firmware section provides a detailed description of the custom network design for the target application.

The Wireless Artificial Vision PV System is presented in Fig. 1. It is divided into two parts: the Wireless Distributed Photovoltaic System (WDPS) and the Wireless Webcam Centralized Control (WWCC). The WWCC consists of a coordinator node connected to a low-cost webcam and a Raspberry Pi. The WDPS includes the PV modules, the buck-boost converter and the wireless sensor network node. The WDPSs and

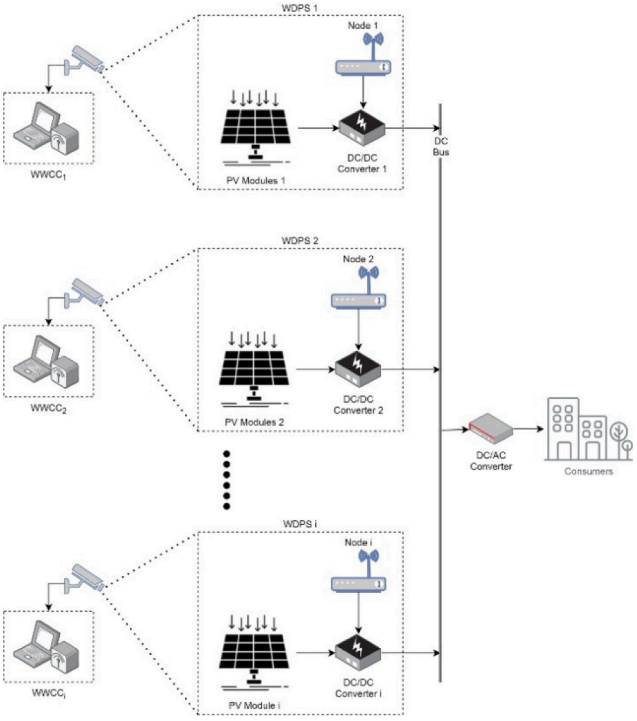


**Fig. 1.** The Wireless Artificial Vision PV System Architecture.

WWCCs form a distributed system that generates electricity to supply the loads. The different PV arrays are supervised by different webcams to guarantee the detection of partial shading conditions and the search of the MPP. Then, the WDPSs are connected to the direct current (DC) bus to convert the DC current to alternating current (AC) current through a DC/AC converter.

### 2.1. Wireless distributed photovoltaic system

The WDPS is made up of the PV system (the PV modules and a DC/DC converter) and the sensor network node. The energy generated by the PV modules is transferred to a buck-boost converter, which is connected to the sensor node. The sensor node is the responsible for reading the sensors, sending the data to the coordinator node, and receiving the control signal to apply to the pulse width modulation (PWM) module.

#### 2.1.1. PV system

The PV system consists of three series-connected PV systems and the buck-boost converter. The PV modules used are commercial, with a peak power of 20.1 W at standard conditions (1000 W/m$^2$ and 25 °C). Thus, the open-circuit voltage is 21.6 V, the short-circuit current is 1.28 A, whereas the voltage and current values for the maximum power are 17.5 V and 1.15 A, respectively. Fig. 2 shows the behaviour of the PV modules for different partial shading conditions.

When there are nonuniform conditions, the P-V curves present multiple peaks. The number of peaks for the three series-connected PV modules ranges from one to three, as Fig. 2 depicts, taking into account that each PV module is connected to a bypass diode. There will be one peak for uniform conditions, and three peaks when each PV module is subjected to a different value of irradiance and/or temperature.

Then, the PV modules feed the buck-boost converter. The DC/DC converter transforms the voltage from one level to another, higher or lower than its input. Usually, in PV systems, the boost converter is used to step up the voltage, but the buck-boost converter is preferred in this work because it can also step down the voltage to feed telecommunication applications. Then, the solar modules output voltage is controlled by means of the buck-boost converter, by varying the duty cycle. Thus,

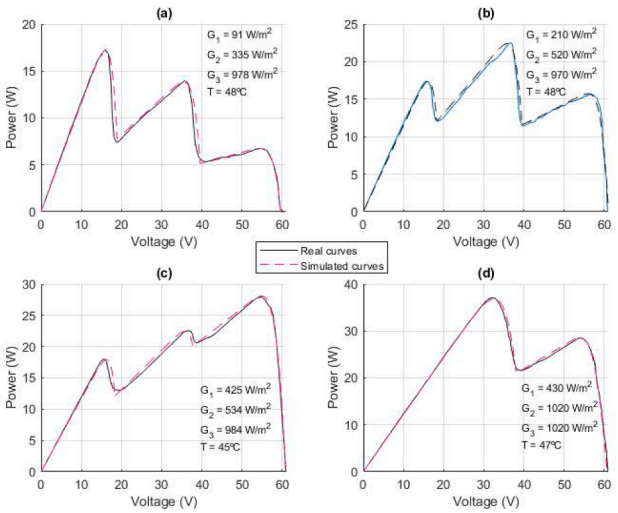


**Fig. 2.** P-V curves under different partial conditions ($G_x$ irradiance, $T_x$ temperature).

the MPP can be reached under all conditions applying the artificial vision algorithm. The built DC/DC converter is able to transfer 70 W. The input voltage ranges from 10 V to 70 V and the maximum output voltage is 100 V. The buck-boost converter has an efficiency higher than 92%, [15].

### 2.1.2. Sensor network node

A WSN is made up of a number of sensor nodes that communicate their readings wirelessly. These nodes are usually small and inexpensive, and have low power requirements. As the information to be gathered for the application in this work is quite exhaustive, several simple sensors are required. For this reason, the information flow becomes critical, so the communication protocol must be adapted to meet the constraints. For each PV panel, a sensor network node with several sensors will be attached to monitor its performance. Apart from the sensors, the nodes also include a processor, a radio system, and a power supply to provide the energy required by the node for its operation.

The WSN developed in this work enables the monitoring of key parameters for the identification of efficiency features, and provides the control commands to track the MPP, further ensuring the stability of the algorithm. Through this network, real-time monitoring of electrical characteristics, and ambient parameters for each panel, is carried out.

In order for the system to perform correctly as a whole, it has to collect the relevant information from the modules attached to each solar cell and transmit it to the coordinator or central node, thus relying on the correct operation of each of these modules. The energy used to power the modules is supplied by the solar panel they are attached to, so they must have guaranteed low power consumption. A wireless sensor network node, which is in charge of measuring relevant magnitudes in each module and transmitting the information to the coordinator node, is included for each module. This later node is located in the supporting structures of the solar modules. The wireless sensor network nodes include sensors and specific circuitry for data transmission. The energy to power the nodes comes from the solar panels, with an additional battery to supply the required power when the PV generation is insufficient. The communication between the wireless sensor network nodes and the coordinator node is enabled by the IEEE 802.15.4 standard using a dual-processor architecture based on two 8-bit microcontrollers from Atmel: the ATmega328P gathers the data from the sensors, and the ATmega128RFA1 handles the wireless communication stack. The dual processor design allows the tasks to be shared between both microcontrollers, achieving real-time monitoring and stable operation of the control algorithm. The measurements of current are carried out with resistors in the board, and voltage dividers for the required measurements of voltages. All these analog values are periodically sampled by an external differential analog to digital converter (ADC). Fig. 3 shows the hardware design of the wireless sensor network node. The wireless sensor node designed exhibits a very low power consumption since it has been optimized by a proper choice of low power hardware components, as well as being optimized at software level by the customized wireless solution as it is described in section III. Thus, the power consumption of the sensor node represents a very low percentage of the total power delivered by the photovoltaic module.

Fig. 4 presents the signal flow of the sensor network node. The sensor node has a 16-bit analog to digital converter to read the sensors measurements. The required signals are the buck-boost converter input voltage, $v_{in}$, and current, $i_{in}$, the DC/DC converter inductor current, $i_L$, the buck-boost converter output voltage, $v_o$, and the temperature, $T$. These values are sampled every 10 ms and sent to the coordinator node to calculate the control signal, the duty cycle of the DC/DC converter, $D_{conv}$. In addition, the control signal is received with a frequency of 100 Hz, taking into consideration the partial shading conditions to reach the MPP. The duty cycle is applied to a PWM module to generate the 10 kHz signal used to switch the DC/DC converter MOSFET.

## 2.2. Wireless webcam centralized control

The WWCC is made up of the coordinator node, the low-cost webcam, and the Raspberry Pi, which is the responsible for the image processing and the DC/DC converter artificial vision control.

### 2.2.1. Webcam and Raspberry Pi

The low-cost webcam used in this work, which costs less than 25$, has 8 MP and a video resolution of 820x640 pixels, guaranteeing a frame rate of 90 fps. After processing the image, a value of 25 fps is obtained. The webcam has a Camera Serial Interface (CSI) port connection.

The Raspberry Pi is a low-cost computer, which costs less than 30$, and where the calculations of the controller are carried out. The Raspberry Pi features a quad-core 64 bits Central Processing Unit (CPU) running at 1.4 GHz, 1 GB of random access memory (RAM), and wireless connectivity. It also has 40 input/output General Purpose Input/Output (GPIO) pins and a universal serial bus (USB) 2.0 port to connect the webcam, guaranteeing a data transfer of 300 Mbps. The Raspberry Pi operating system is Linux Raspbian whereas the artificial vision software is Open Source Computer Vision Library (OpenCV). The Raspberry Pi is the responsible for running the artificial vision algorithm, obtaining the reference voltage for the MPP under all environmental conditions.

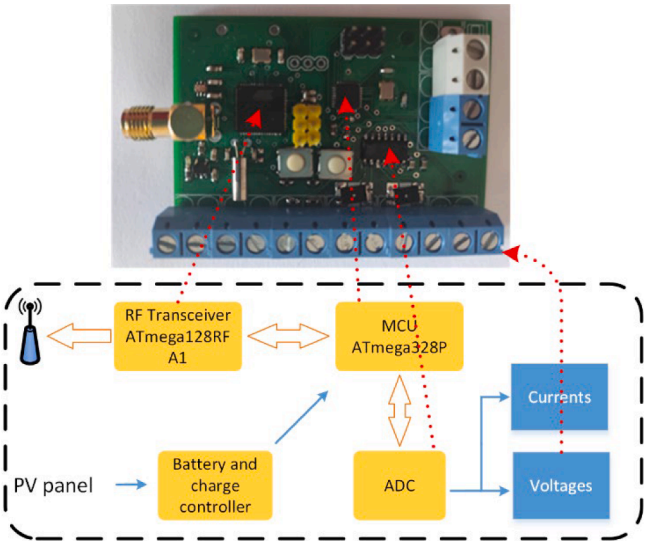


**Fig. 3.** Architecture of the proposed IEEE 802.15.4 wireless network node.

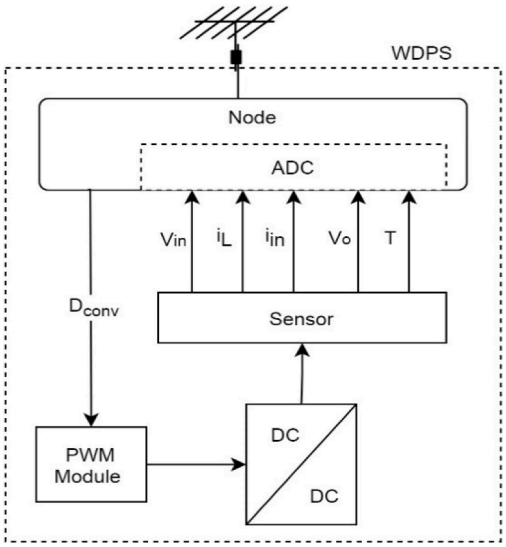


**Fig. 4.** Sensor network node signal flow.

Besides, it is responsible for calculating the control signal, i.e., the duty cycle of the buck-boost converter, by means of a backstepping controller.

### 2.2.2. Partial shading conditions MPPT

The artificial vision algorithm uses a webcam to identify the partial shading that affects the PV modules. For that, two parameters are defined, the shadow intensity and the shadow irradiance. The shadow intensity, $I_{sPVj}$, is the average value of grey level of the pixels included in a blob area, and it is obtained from to the images received by the webcam. When the shadow intensity is zero, the PV modules are unshaded, and the maximum value that the shadow intensity can reach is 100 (the maximum level of darkness). Then, taking into account the shadow intensity, the shadow irradiance, $G_{sPVj}$, can be calculated as Eq. (1). Thus, each PV module has a shadow irradiance value.

$$G_{sPVj} = \widehat{G}e^{-\left(0.0306I_{sPVj}\right)} \tag{1}$$

where $j$ is the number of solar modules and $\widehat{G}$ is an estimated irradiance [53].

The proposed artificial vision algorithm uses C language and open sources libraries, such as "opencv" and "cvblob". The algorithm has to select the shaded images (region of interest, ROI) to convert them to Hue-Saturation-Value (HSV) color format. Then, a segmentation process is required, including the HSV thresholding to select the threshold for the shadow, the morphology transformation to filter the noise, and the blob detection to identify the minimum area affected by the shadow. Thus, the shadow irradiance is obtained. Finally, with the calculated shadow irradiance and the measurements of the temperature, the PV modules output voltage, and current, the reference voltage to reach the MPP under partial shading conditions is obtained [30], avoiding the local maxima. This reference voltage is later used by the backstepping controller to regulate the DC/DC converter input voltage.

After applying the artificial vision algorithm, the controller used for the buck-boost converter is a nonlinear backstepping controller [15]. This controller is able to guarantee the robustness and stability of the system thanks to Lyapunov functions, globally positive-definite functions with negative time derivatives, which ensures a global asymptotically stable solution. The Lyapunov functions have the next form: $V_i=(1/2)e_i^2$, where $e_i$ is the defined error in each case. In this paper, the errors are $e_1$, which is the voltage error, and $z_1$, the inductor current error, [15]. For both cases the errors are defined as the difference between the measured values and the references. Then, the control signal, the duty cycle, is used to regulate the DC/DC converter input voltage to ensure that the PV modules work at the MPP under all conditions. In this way, the artificial vision generates the reference voltage that provides the MPP, and this voltage is required by the backstepping control. The operation of the controller requires having an inner control loop for the inductor current, and an outer loop for the PV modules output voltage. Then, an inductor reference current is generated to be used by the inner loop whereas the control signal is generated by the current inner loop [15].

To use the backstepping control method and stabilize the DC/DC converter to the origin, the buck-boost converter dynamics are used, Eqs. (2) and (3), where $i_L$ is the inductor current.

$$\dot{v}_{in} = \frac{i_{in} - i_L D_{conv}}{C_1} \tag{2}$$

$$\dot{i}_L = \frac{v_o}{L} + \frac{v_{in} - v_o D_{conv}}{L} \tag{3}$$

The procedure to achieve the control signal requires the application of different steps [15]. First, taking into account (2) and (3), the voltage error time derivative is needed. Then, the Lyapunov function and its time derivative is also required. Thus, the stabilization function (or inductor reference current) is obtained, $\alpha 1 = (C_1 k_1 e_1 + i_{in} - C_1 \dot{v}_{ref})/D_{conv}$, and it is nonzero, where $D_{conv}$ ($0 < D_{conv}$ less than 1) is the duty cycle, $v_{ref}$ is the reference buck-boost converter input voltage, and $k_1$ is a positive constant. After that, considering the stabilization function, the process is repeated adding the inductor current error time derivative. Now, the Lyapunov function time derivative includes the voltage error and the inductor current error. Finally, working out the time derivative of the duty cycle from the time derivative of the Lyapunov function, the control signal is obtained in Eq. (4).

$$\dot{D}_{conv} = \frac{1}{\alpha_1}\left(-\frac{v_0}{L}D_{conv} - \frac{v_{in} - v_0}{L}{D_{conv}}^2 - e_1\left(C_1 k_1^2 - \frac{{D_{conv}}^2}{C_1}\right) + z_1(k_1 - k_2)D_{conv} - C_1\ddot{v}_{ref} + \dddot{i}_{in}\right) \tag{4}$$

where $L$ is the inductor, $C_1$ is the capacitor, and $k_2$ is a positive constant.

### 2.2.3. Coordinator node

In the implementation of the network that enables the recollection of data from all the PV modules, a star-structure using IEEE 802.15.4 modules was chosen. The wireless system is governed by the coordinator node, which is attached to the central computer (Raspberry Pi) in charge of data storage, visualization of relevant information from the whole network, image processing, and the DC/DC converter artificial vision control. Fig. 5 shows the board of the coordinator node. It includes the 8-bit ATmega128RFA1 microcontroller. The coordinator node is powered from the Raspberry Pi, and is connected directly to it. Just like in the sensor node, an antenna has been connected through a SubMiniature version A (SMA) connector.

Fig. 6 presents the signal flow of the coordinator node. The webcam is connected to the Raspberry Pi, and the Raspberry Pi is connected to the coordinator node. The coordinator node receives the sensor data, $v_{in}$, $i_{in}$, $i_L$, $v_o$ and $T$, that are sent by the sensor network node every 10 ms. The artificial vision algorithm requires the values of $v_{in}$, $i_{in}$, $T$, and the webcam images that are sent at a rate of 25 fps. Thus, the reference voltage, $v_{ref}$, that provides the MPP under partial shading conditions, is calculated. Then, using the reference voltage and the sensor measurements of $v_{in}$, $i_{in}$, $i_L$ and $v_o$, the control signal, $D_{conv}$, is obtained by means of a backstepping controller. Finally, the control signal is sent by the coordinator node to the sensor network node with a sample time of 10 ms.

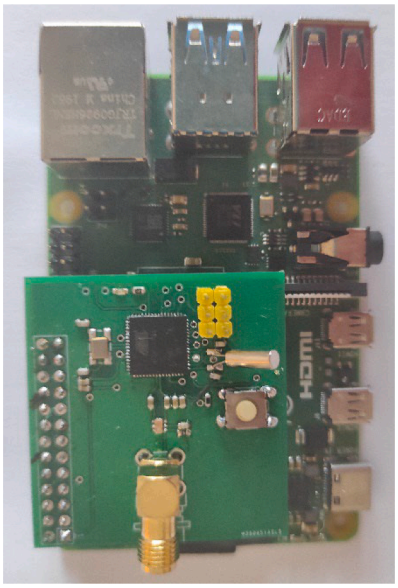

**Fig. 5.** Image of the coordinator node connected to the Raspberry Pi (placed at the bottom).

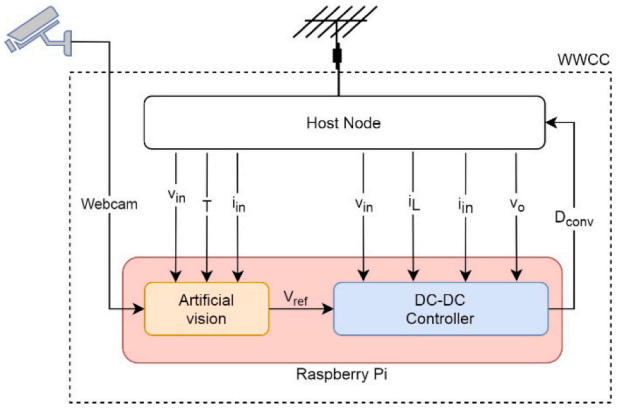


**Fig. 6.** Coordinator (host) node signal flow.

## 3. Firmware

In the IEEE 802.15.4 standard, the specification for the MAC protocol for sensor nodes provides two modes of operation: an asynchronous, beaconless mode, and a synchronous, beacon-enabled one. In the beaconless mode, the nodes must always be listening for possible transmissions from other devices, which can have a great impact on battery life. This asynchronous approach requires for the nodes to be almost continuously in receive mode, awaiting data from the other devices in the network. Channel access is managed through an unslotted carrier-sense multiple access with collision avoidance (CSMA/CA) protocol. In contrast, the beacon-enabled mode provides a synchronous approach for the transmission of data between transmitter and receiver.

The choice in this work was the beacon-enabled mode, as synchronization allows devices to sleep between transmissions, with coordination resulting in energy savings and, consequently, prolonged network battery life. The access to channel and the transmission of data are carried out using a superframe structure. The coordinator decides the superframe structure considering the beacon interval (BI), which indicates the time interval between two consecutive beacon frames, as well as the superframe duration (SD), indicating the time a node is active during the BI. As part of the superframe there is a contention access period (CAP) during which all the devices in the network gain access and compete for time slots using a slotted CSMA/CA protocol, followed by a contention free period (CFP), which is divided into guaranteed time slots (GTSs) that get allocated by the coordinator, for low latency applications. As a mechanism for reducing energy consumption, an inactive period can be introduced by the coordinator by choosing BI $>$ SD. During this inactive period all devices in the network, including the coordinator, enter sleep mode. Two parameters determine BI and SD, namely the beacon order (BO) and the superframe order (SO) [54]. A minimum superframe duration of 15.36 ms corresponds to SO $=$ 0, assuming a 250 Kbps data rate in the 2.4 GHz frequency band.

According to the above description, Atmel microcontrollers govern both sensor and coordinator nodes. The layered approach of the Atmel MAC architecture is based upon several stack modules that enable the mechanisms and functionalities of the 802.15.4 standard for wireless transceivers. Among them, the modules that have been adapted to the target application requirements, are the followings:

- Platform Abstraction Layer (PAL): provides interfaces to timers, GPIO control (access from microcontroller to the general purpose I/O pins connected to the transceiver), low-level interrupt handling, serial I/O support, and access to storage.
- The MAC module: includes the protocol stack of the 802.15.4 communications standard; within this module we must highlight the MAC-API, which is the stack for specific applications.
- Transceiver Abstraction Layer (TAL): contains the transceiver specific functionality.
- Resources: includes the management of buffers and ~~the~~ queues.

The main MAC stack firmware consists of three layers starting from the bottom up: PAL, TAL and MAC Core layer (MCL).

The PAL contains all platform (that is, microcontroller unit (MCU) and board) specific functionality and provides interfaces to the upper modules. For each microcontroller a separate implementation exists within the PAL layer. The board and application needs are adapted via a board configuration file. The PAL provides interfaces to timers, GPIO control (access from microcontroller to the general purpose I/O pins connected to the transceiver), low-level interrupt handling, serial I/O support and access to storage.

The TAL contains the transceiver specific functionality used for the 802.15.4 MAC support and provides interfaces to the MAC Core Layer, which is independent from the underlying transceiver. Components implemented in this layer are the frame transmission unit to generate and transmit the frames, the frame reception unit to read and upload the incoming frames including automatic acknowledgement handling, the state machine, or the CSMA/CA module for channel access, power management, and initialization and reset.

The MCL abstracts and implements IEEE 802.15.4 compliant behavior for beacon-enabled network support. The application interfaces the MAC stack via the implemented MAC-API building block. It sends requests and responses to the stack by calling the functions provided by the MAC-API. It also invokes the confirmation and indication callback functions implemented by the user. Moreover, the Beacon Manager generates the beacon frames, which are transmitted using the TAL, and is also responsible for beacon reception at the start of a superframe and its synchronization. The received beacons are processed based on the current state of the MAC and, if required, indications or notifications are given to the MAC-API.

The last stack module that has been used is the Resource Management. It provides access to resources to the stack or to the application. The resources are the buffer management for dynamically allocating and freeing memory buffers, and the queue management for creating and maintaining the queues.

Figs. 7 and 8 show the flow diagrams of the sensor and coordinator nodes, respectively. In Fig. 7, the sensor node (end device) first tries to send an association frame, in order to associate with the network. This process is also known as broadcast, and is defined within the standard as

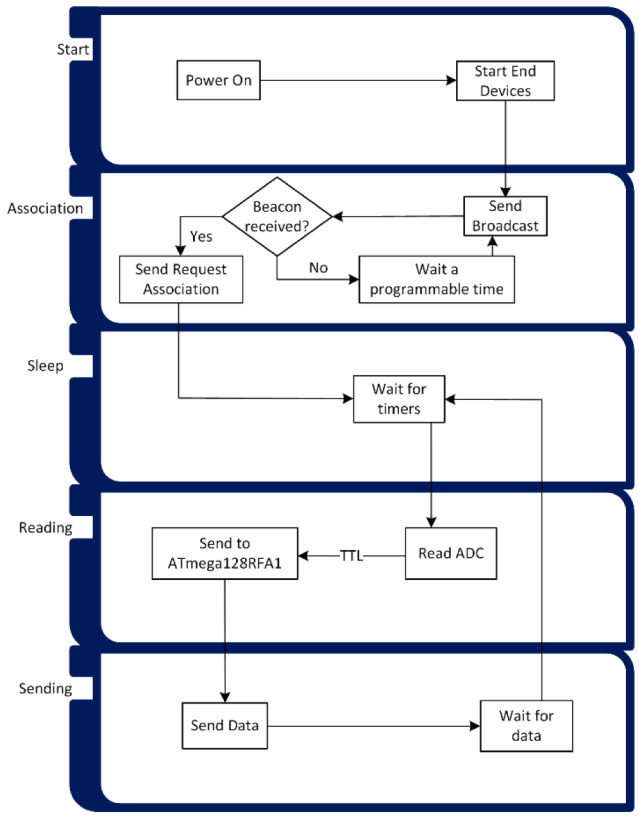


**Fig. 7.** Flow diagram of the sensor network node.

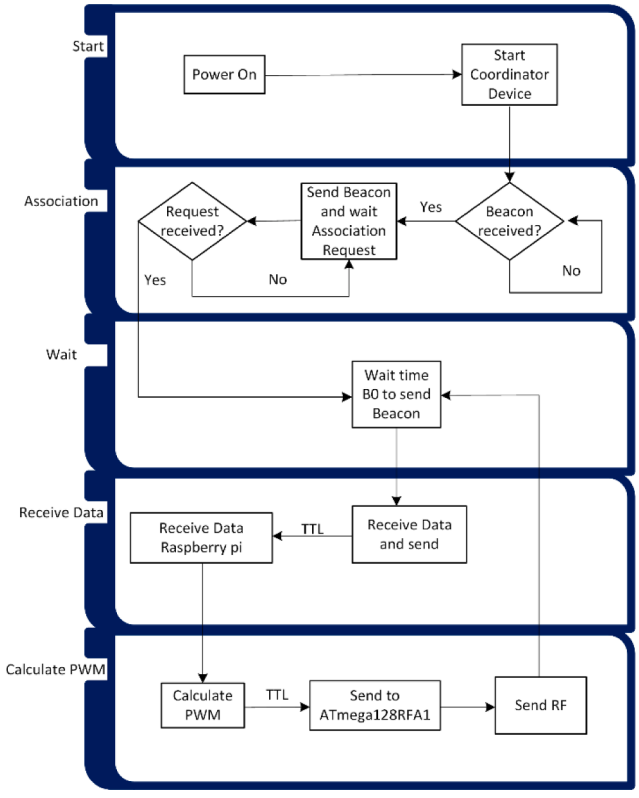


**Fig. 8.** Flow diagram of the coordinator node.

association beacon. When the sensor node receives the response from the coordinator, it accepts the association. Following this step, the sensor node switches its ADC from sleep to active mode, and takes a data reading. Next, by means of the ATmega128RFA1 RF transceiver, the data is transmitted to the coordinator node, and the ADC is once more switched to sleep mode, reducing its energy consumption. The procedure is completed once the data is successfully sent to the coordinator node, after which the sensor node will wait for the reception of a new beacon so as to repeat the aforementioned procedure.

In Fig. 8, the coordinator node first configures the parameters required to create the network, from which point it will wait for any of the sensor nodes to send it a beacon. When an initial broadcast is received, which equates to an association beacon having been sent by a sensor node, a PV module number is associated by the coordinator node to the MAC address of the sensor node, followed by the coordinator broadcasting an association beacon, and waiting for the response from the sensor node. When the confirmation of association agreement is received from the sensor, its address is already buffered by the coordinator. Next, after waiting for a time interval defined by the BO and SO parameters, the coordinator sends a data request beacon. Two events can occur after this beacon is sent: either an acknowledgement from the sensor node is be received by the coordinator, which means that the sensor node has already been associated, so the data gets sent to the base station, or, in the opposite case, the coordinator receives no data from the sensor note, so it sends another data request beacon.

## 4. Experimental validation

Fig. 9 presents the experimental platform used to carry out a set of experiments. Fig. 9 a) shows the shaded PV modules whereas Fig. 9 b) depicts the equipment: (a) is the PV modules connection, (b) is the buck-boost converter output to the load in this case, (c) is the sensor network

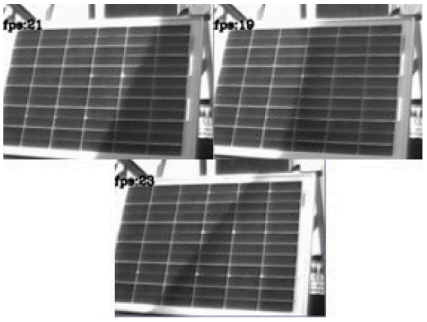

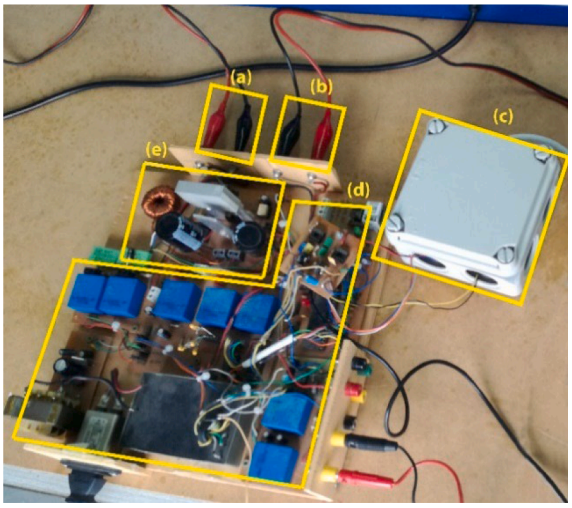


**Fig. 9.** Experimental platform.

node, (d) are the sensors and (e) is the buck-boost converter.

Different partial shading conditions have been provided in the experiments to verify the correct operation of the system. For that, the incident irradiance onto the solar modules has been modified to work under different non-uniform environmental conditions.

Fig. 10 shows the evolution of the shadow intensity, $I_{sPVx}$, and the shadow irradiance, $G_{sPVx}$. Fig. 10 a) presents the shadow intensity, which is given as a percentage. There are three signals because each PV module can be affected by different irradiance. Thus, in the first interval, from 0 s to 13 s, all the solar modules are affected by different shadows. In the second interval, from 13 s to 40 s, only two PV modules, 1 and 2, are partially shaded with different irradiances, whereas the solar module number 3 has a value of zero, which means that the PV module is unshaded. In the third interval, that ranges between 40 s and 58 s, the PV modules 2 and 3 are unshaded whereas the PV module 1 is partially shaded. Finally, in the last interval, from 58 s to 85 s, there are again two partially shaded modules with different irradiance (1 and 2) and another unshaded solar module. Thus, for the time that the experiment lasts, the PV module 1 is partially shaded with almost constant irradiance, the PV module 2 is affected by an intermittent shadow, whereas the PV module 3 is only affected by partial shadows in the first time interval.

Fig. 10 b) depicts the shadow irradiance, which is calculated taking into consideration the shadow intensity given by Eq. (1). When the shadow intensity is equal to 0 %, the shadow irradiance is 1000 W/m$^2$. The different values for the relationship between the shadow intensity and the shadow irradiance are summarized in Table 1. For the interval that ranges from 40 s to 58 s, a two-peak P-V curve is achieved since different irradiances are incident on the PV modules (unshaded modules with 1000 W/m$^2$ for the PV modules 2 and 3, and a partially shaded solar module with 210.5 W/m$^2$ for the PV module number 1). The other intervals present a three-peak P-V curve because there are three different levels of irradiance. All these results are summarized in Table 1.

The P-V curves from the different intervals are presented in Fig. 11. In (a), (b) and d) there are three-peak P-V curves because there are three different values of irradiances (shaded and unshaded PV modules) whereas in c) there is a two-peak P-V curve because there are two different values of irradiance with only one shaded PV module.

Fig. 12 presents the DC/DC input power and the reference power or MPP. The powers achieved in each interval are 4.4 W, 16.1 W, 39.69 W and 17.2 W, respectively. As it shows, the reference power is reached in all the cases. Thus, for the artificial vision MPPT tracking efficiency, the relationship between the DC/DC converter input measured power, $P_{in}$, and the reference power, $P_{ref}$, ranges from 98.2 % to 99.3 %. In addition, for the buck-boost converter efficiency, the relationship between the DC/DC converter input and output power, ranges from 97.9 % to 98.3

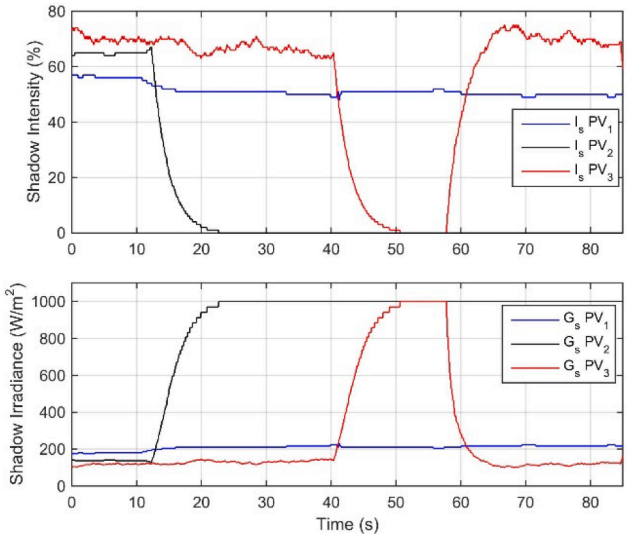


**Fig. 10.** Evolution of the shadow intensity and shadow irradiance.

**Table 1**
Shadow intensity and shadow irradiance.

| Interval (s) | [0–13) | [13–40) | [40–58) | [58–85) |
|---|---|---|---|---|
| $I_{sPV1}$ (%) | 52 | 50 | 51 | 50 |
| $I_{sPV2}$ (%) | 64 | 0 | 0 | 0 |
| $I_{sPV3}$ (%) | 68 | 66 | 0 | 74 |
| $G_{sPV1}$ (W/m$^2$) | 197.5 | 210.2 | 210.5 | 210.8 |
| $G_{sPV2}$ (W/m$^2$) | 141.1 | 1000 | 1000 | 1000 |
| $G_{sPV3}$ (W/m$^2$) | 128.8 | 141.3 | 1000 | 107.2 |

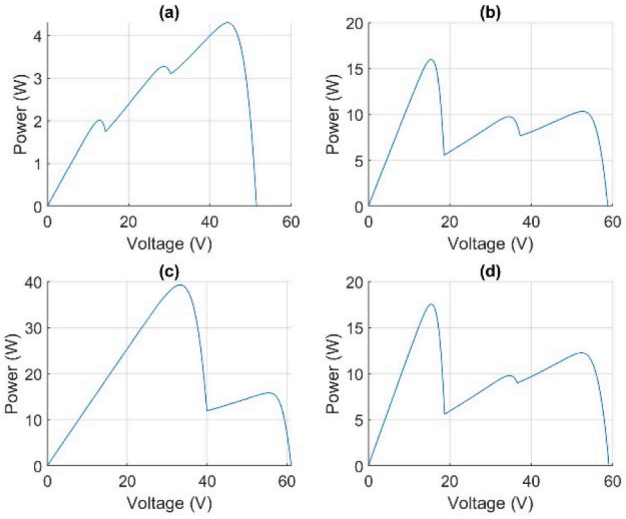


**Fig. 11.** P-V curves for the different time intervals.

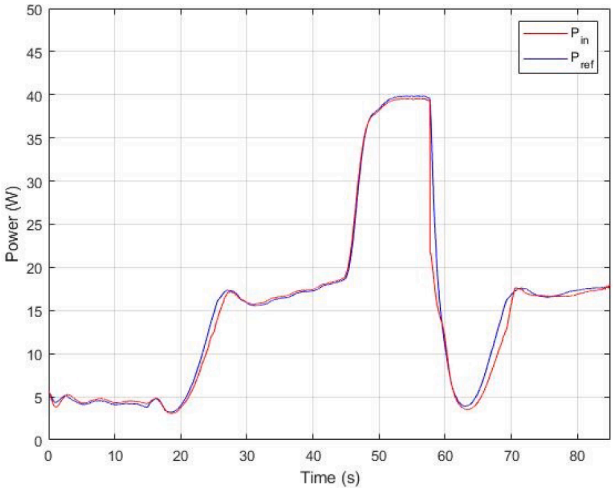


**Fig. 12.** Evolution of power under partial shading conditions.

**Table 2**
MPPT algorithm results.

| Interval (s) | [0–13) | [13–40) | [40–58) | [58–85) |
|---|---|---|---|---|
| No. of peaks | 3 | 3 | 2 | 3 |
| $v_{in}$ (V) | 44.9 | 13.2 | 32.7 | 14.6 |
| $P_{ref}$ (W) | 4.40 | 16.10 | 39.69 | 17.20 |
| $P_{in}$ (W) | 4.37 | 15.90 | 38.98 | 17.00 |
| $P_{real}$ (W) | 4.41 | 16.12 | 39.71 | 17.21 |

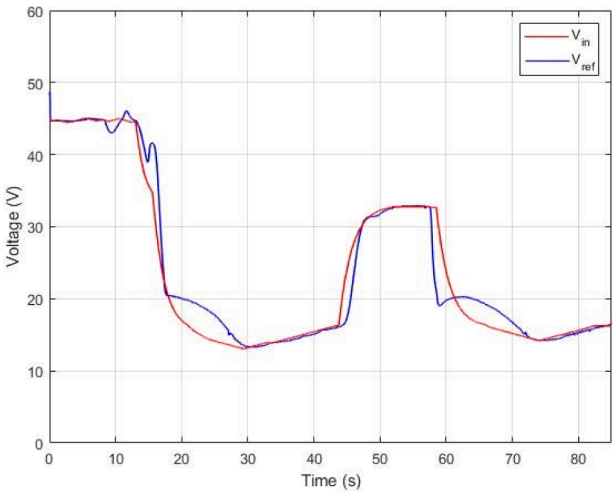


**Fig 13.** Evolution of voltage under partial shading conditions.

%. These results are summarized in Table 2.

Fig. 13 depicts the buck-boost converter input voltage (or the PV modules output voltage) and the reference voltage that provides the MPP (it is given by the artificial vision algorithm and it has to be tracked by the backstepping controller). In the first interval, when the three solar modules are partially shaded, the voltage obtained is 44.9 V. In the second and fourth intervals, when there are two partially shaded PV modules and one unshaded solar module, the voltages obtained are 13.2 V and 14.6 V, respectively. Finally, in the third interval, when there is only one partially shaded PV module, the voltage reached is 32.7 V. This figure also shows that the reference voltage is properly tracked, achieving a high control efficiency. These results are also summarized in Table 2. This table also presents the value of the real MPP that has to be reached, $P_{real}$, to compare this value with the power measured at the PV modules output, $P_{in}$, and the predicted power given by the algorithm through the WSN, $P_{ref}$.

Fig. 14 depicts the control signal, i.e., the duty cycle of the buck-boost converter. The control signal is changing when the different irradiances occur, to achieve the MPP under all conditions. In addition, the figure shows that the signal is smooth, and the response of the remote controller does not have oscillations when there is a change, verifying that the controller is robust even operating through a wireless sensor network.

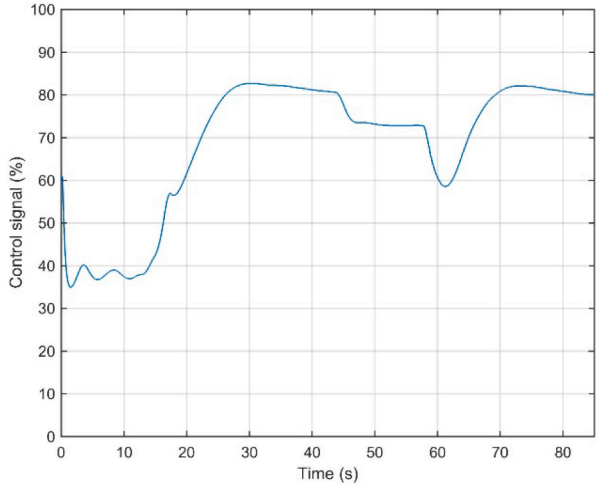


**Fig. 14.** Evolution of control signal under partial shading conditions.

## 5. Discussion and comparison

The experimental results prove the correct operation of the MPPT artificial vision algorithm in PV systems even working under partial shading conditions and through a WSN. The algorithm efficiency remains high, between 98.2 % and 99.3 %, whereas the DC/DC converter efficiency is not affected, achieving a high value as well, between 97.9 % and 98.3 %. Thus, the MPP is always reached under all circumstances, no matter the number of peaks on the P-V curve and the number of PV modules unshaded, shaded, or partially shaded.

Looking at Fig. 12, the efficiency can be calculated, and it shows that the highest efficiency, 99.3%, is obtained when the power is lower, whereas the lowest efficiency, 98.2%, is obtained when the power is higher. Even so, the lower efficiency is appropriate for the system.

Regarding Fig. 13, the reference voltage given by the artificial vision algorithm is always tracked by the DC/DC converter input voltage. The reference values are reached quickly even when applying sudden changes in the system.

Finally, Fig. 14 depicts the evolution of the control signal taking into consideration the experiment carried out, where the PV modules are affected for three different values of irradiance, except from the interval from 40 s to 58 s where the P-V curve presents a two-peak curve. Considering all these changes and the wireless controller, the evolution of the control signal is smooth with no oscillations, proving the system is stable and robust.

A comparison of the proposed algorithm's performance with other recent state-of-the-art techniques is given Table 3. From the results, it can be seen that the proposed algorithm offers very high efficiency, moderate computation effort, medium complexity, and a low cost hardware implementation. It also offers the advantages of being stable and robust regardless the environmental conditions and the partial shading conditions. In addition, this algorithm can be used in a wireless sensor network preserving the same features, since the wireless network implements a mechanism which guarantees that the data is sent with a latency such that the controller can work stably.

## 6. Conclusions

In this paper are addressed important aspects regarding PV systems and wireless sensor networks, considering a combination of the two that transforms the classical PV installation into a smart PV system. That is, the application of wireless sensor and actuator networks and communication protocols in PV systems becomes a promising solution that makes them more intelligent. Fundamental characteristic of the IEEE 802.15.4 standard, such as low-cost, easiness of deployment, high flexibility, fault-tolerance, or low power consumption make it a suitable solution for the proposed smart PV monitoring and control system. The adapted MAC layer of the 802.15.4 protocol provides a balance between a high-quality radio resource and energy requirements in the target application. Improved energy efficiency in the MAC layered is obtained by adopting a synchronous duty cycling strategy, which allows for efficient, coordinated sleep/wakeup schedules for the nodes. The energy savings achieved far outweigh the coordination cost. The use of microcontrollers and communication technologies in the development of WSNs can improve the current methods of monitoring and control, supporting the appropriate real-time response in PV power generation.

## CRediT authorship contribution statement

**Aranzazu D. Martin:** Conceptualization, Formal analysis, Investigation, Methodology, Supervision, Writing – original draft. **Juan M. Cano:** Data curation, Investigation, Resources, Validation. **Jonathan Medina-García:** Data curation, Resources, Validation. **Juan A. Gómez-Galán:** Formal analysis, Methodology, Writing – review & editing. **Adoración Hermoso:** Project administration, Software. **Jesus R. Vazquez:** Project administration, Visualization.

**Table 3**
Comparative of recent techniques of MPPT implementations.

| Reference | Specific type of MPPT controller | Hardware/software platform | DC-DC converter | Solar panel | MPPT time (s) | MPPT efficiency (%) | Computation effort |
|---|---|---|---|---|---|---|---|
| [17] | EA-P&O | TMS320F240 DSP/ dSPACE | Buck-boost | Simulated MSX60 modules (PVAS) | 0.25 | 99 | Moderate |
| [25] | FL | TMS320F28335 DSP/ PSIM | Boost | 75 W simulated PV module | 0.01 | >99 | Moderate |
| [26] | FL | FPGA and MATLAB/ Simulink | Boost | 60 W solar panel | 0.3 | 98.00 | Moderate |
| [28] | ANN | MATLAB/ Simulink | | Simulated | 0.2–0.4 | > 90 | High |
| [31] | PSO | MC56F8245 micro-processor | Buck | TC.P.32 PV simulator 1000 V/13 A | ±1.6 | 97.00 | Moderate |
| [32] | Hybrid (P&O-ANN and IC-ANN) | MATLAB/ Simulink | Cuk | SHARP 80 W | ±0.400 | >91.0 | High |
| [38] | Hybrid (ANFIS-PSO) | MATLAB/ Simulink linked to dSPACE DS1104 board | Zeta | | ±0.300 | 98.35 | High |
| [39] | ANFIS | FPGA and MATLAB/ Simulink | Buck | 60 W PV module | 0.012 | 91.0 | High |
| [41] | ML | MATLAB/ Simulink | Boost | 250 W PV module | ±1.88 | 98.4 | High |
| This work | Backstepping and vision | Raspberry Pi | Buck-boost | 20 W PV module | 0.32–0.91 | 99.30 | Moderate |

## Declaration of Competing Interest

The authors declare that they have no known competing financial interests or personal relationships that could have appeared to influence the work reported in this paper.

## Data availability

The data that has been used is confidential.

## References


[1] UrRehmana O, Khan SA, Javaid N. Impact of photovoltaic self-consumption curtailment on building-to-grid operations. Int J Electr Power Energy Syst 2021; 124:106374.
[2] Xia K, Ni J, Ye Y, Xu P, Wang Y. A real-time monitoring system based on ZigBee and 4G communications for photovoltaic generation. CSEE J Power Energy Syst 2020;6(1):52–63.
[3] Sun X, Su Y, Huang Y, Tan J, Yi J, Hu T, et al. Photovoltaic modules monitoring based on WSN with improved time synchronization. IEEE Access 2019;7: 132406–12.
[4] Le PT, Tsai HL, Lam TH. A wireless visualization monitoring, evaluation system for commercial photovoltaic modules solely in MATLAB/Simulink environment. Sol Energy 2016;140:1–11.
[5] Moon S, Kim SJ, Seo JW, Park JH, Park C, Chung CS. Maximum power point tracking without current sensor for photovoltaic module integrated converter using Zigbee wireless network. Electr Power Energy Syst 2014;56:286–97.
[6] Llaria A, Terrasson G, Curea O, Jiménez J. Application of wireless sensor and actuator networks to achieve intelligent microgrids: A promising approach towards a global smart grid deployment. Appl Sci 2016;6(3):61.
[7] Moreno-Garcia IM, Palacios-Garcia EJ, Pallares-Lopez V, Santiago I, Gonzalez-Redondo MJ, Varo-Martinez M, et al. Real-time monitoring system for a utility-scale photovoltaic power plant. Sensors 2016;16(6):770.
[8] IEEE Standard for Low-Rate Wireless Networks (2020, Jul.). https://standards.ieee.org/standard/802_15_4-2020.html.
[9] Killi M, Samanta S. Modified perturb and observe MPPT algorithm for drift avoidance in photovoltaic systems. IEEE Trans Ind Electron 2015;62(9):5549–59.
[10] Alsumiri M. Residual incremental conductance based nonparametric MPPT control for solar photovoltaic energy conversion system. IEEE Access 2019;7:87901–6.
[11] Barth C, Robert CN, Pilawa-Podgurski N. Dithering digital ripple correlation control for photovoltaic maximum power point tracking. IEEE Trans Power Electron 2015;30(8):4548–59.
[12] Salem Elbarbary ZM, Alranini MA. Review of maximum power point tracking algorithms of PV system. Front Eng Built Environ 2021;1(1):68–80.
[13] Cortajarena JA, Barambones O, Alkorta P, Cortajarena J. Sliding mode control of an active power filter with photovoltaic maximum power tracking. Int J Electr Power Energy Syst 2019;110:747–58.
[14] Bag A, Subudhi B, Kumar RP. A combined reinforcement learning and sliding mode control scheme for grid integration of a PV system. CSEE J Power Energy Syst 2019;5(4):498–506.
[15] Martin AD, Cano JM, Silva JFA, Vazquez JR. Backstepping control of smart grid-connected distributed photovoltaic power supplies for telecom equipment. IEEE Trans Energy Convers 2015;30(4):1496–504.
[16] Correa-Betanzo C, Calleja H, Aguilar C, et al. Photovoltaic-based DC microgrid with partial shading and fault tolerance. J Mod Power Syst Clean Energy 2019;7(2): 340–9.
[17] Ahmed J, Salam Z. An enhanced adaptive P&O MPPT for fast and efficient tracking under varying environmental conditions. IEEE Trans Sustain Energy 2018;9(3): 1487–96.
[18] Kouchaki A, Iman-Eini H, Asaei B. A new maximum power point tracking strategy for PV arrays under uniform and non-uniform insolation conditions. Sol Energy 2013;91:221–32.
[19] Kai C, Shulin T, Yuhua C, Libing B. An improved MPPT controller for photovoltaic system under partial shading condition. IEEE Trans Sustain Energy 2014;5(3): 978–85.
[20] Tey KS, Mekhilef S. Modified incremental conductance algorithm for photovoltaic system under partial shading conditions and load variation. IEEE Trans Ind Electron 2014;61(10):5384–92.
[21] Yung Yap K, Sarimuthu CR, Mun-Yee LJ. Artificial intelligence based MPPT techniques for solar power system: A review. J Mod Power Syst Clean Energy 2020; 8(6):1043–59.
[22] Dadkhah J, Niroomand M. Optimization methods of MPPT parameters for PV systems: Review, classification, and comparison. J Mod Power Syst Clean Energy 2021;9(2):225–36.
[23] Jiang LL, Srivatsan R, Maskell DL. Computational intelligence techniques for maximum power point tracking in PV systems: A review. Renew Sustain Energy Rev 2018;85:14–45.
[24] Messai A, Mellit A, Guessoum A, Kalogirou SA. Maximum power point tracking using a GA optimized fuzzy logic controller and its FPGA implementation. Sol Energy 2011;85(2):265–77.
[25] Rezk H, Aly M, Al-Dhaifallah M, Shoyama M. Design and hardware implementation of new adaptive fuzzy logic-based MPPT control method for photovoltaic applications. IEEE Access 2019;7:106427–38.
[26] Youssefa A, Telbany ME, Zekry A. Reconfigurable generic FPGA implementation of fuzzy logic controller for MPPT of PV systems. Renew Sustain Energy Rev 2018;82: 1313–9.
[27] Heidari M. Improving efficiency of photovoltaic system by using neural network MPPT and predictive control of converter. Int J Renew Energy Res 2016;6(4).
[28] Chen L, Wang X. An enhanced MPPT Method based on ANN-assisted sequential Monte Carlo and quickest change detection. IET Smart Grid 2019;2(4):635–44.
[29] Chen LR, Tsai CH, Lin YL, Lai YS. A biological swarm chasing algorithm for tracking the PV maximum power point. IEEE Trans Energy Convers 2010;25(2): 484–93.
[30] Koad RBA, Faheem Zobaa A, El-Shahat A. A novel MPPT algorithm based on particle swarm optimization for photovoltaic systems". IEEE Trans Sustain Energy 2017;8(2):468–76.
[31] Li H, Yang D. An overall distribution particle swarm optimization MPPT algorithm for photovoltaic system under partial shading. IEEE Trans Ind Electron 2018;66(1): 265–75.
[32] Vimalarani C, Kamaraj N, Babu BC. Improved method of maximum power point tracking of photovoltaic (PV) array using hybrid intelligent controller. Optik 2018; 168:403–15.
[33] Alajmi BN, Ahmed KH, Finney SJ, Williams BW. Fuzzylogic-control approach of a modified hill-climbing method for maximum power point in microgrid standalone photovoltaic system. IEEE Trans Power Electron 2011;26(4):1022–30.
[34] Al Nabulsi A, Dhaouadi R. Efficiency optimization of a DSP-based standalone PV system using fuzzy logic and dual-MPPT control. IEEE Trans Ind Informat 2012;8 (3):573–84.
[35] Zainuri MAAM, Radzi MAM, Soh AC, Rahim NA. Development of adaptive perturb and observe-fuzzy control maximum power point tracking for photovoltaic boost dc-dc converter. IET Renew Power Gener 2014;8(2):183–94.
[36] Priyadarshi N, Padmanaban S, Maroti PK, Sharma A. An extensive practical investigation of FPSO-based MPPT for grid integrated PV system under variable operating conditions with anti-islanding protection. IEEE Syst J 2018;13(2): 1861–71.
[37] Priyadarshi N, Padmanaban S, Bhaskar MS, Blaabjerg F, Sharma A. Fuzzy SVPWM-based inverter control realisation of grid integrated photovoltaic-wind system with

fuzzy particle swarm optimisation maximum power point tracking algorithm for a gridconnected PV/wind power generation system: Hardware implementation. IET Electr Power Appl 2018;12(7):962–71.
[38] Priyadarshi N, Padmanaban S, Holm-Nielsen JB, et al. An experimental estimation of hybrid ANFIS-PSO-based MPPT for PV grid integration under fluctuating sun irradiance. IEEE Syst J 2019;14(1):1218–29.
[39] Aldair AA, Obed AA, Halihal AF. Design and implementation of ANFIS-reference model controller based MPPT using FPGA for photovoltaic system. Renew Sustain Energy Rev 2018;82:2202–17.
[40] Du Y, Yan K, Ren Z, et al. Designing localized MPPT for PV systems using fuzzy-weighted extreme learning machine. Energies 2018;11:2615–24.
[41] Keyrouz F. Enhanced Bayesian based MPPT controller for PV systems. IEEE Power Energy Tech Syst J 2018;5(1):11–7.
[42] Sundareswaran K, Sankar P, Nayak PSR, Simon SP, Palani S. Enhanced energy output from a PV system under partial shaded conditions through artificial bee colony. IEEE Trans Sustain Energy 2015;6(1):198–209.
[43] Rajani K, Ramesh T. Maximum power enhancement under partial shadings using modified Sudoku reconfiguration. CSEE J Power Energy Syst 2021;7(6):1187–201.
[44] Batzelis EI, Kampitsis GE, Papathanassiou SA, Manias SN. Direct MPP calculation in terms of the single-diode PV model parameters. IEEE Trans Energy Convers 2015;30(1):226–36.
[45] Kang BK, Kim ST, Bae SH, Park JW. Diagnosis of output power lowering in a PV array by using the Kalman-filter algorithm. IEEE Trans Energy Convers 2012;27(4):885:94..
[46] Moghassemie A, Ebrahimib S, Padmanabana S, Mitoloc M, Holm-Nielsen JB. Two fast metaheuristic-based MPPT techniques for partially shaded photovoltaic system. Int J Electr Power Energy Syst 2022;137:107567.
[47] Yin L, Su Z. Multi-step depth model predictive control for photovoltaic power systems based on maximum power point tracking techniques". Int J Electr Power Energy Syst 2021;131:107075.
[48] Kumar N, Singh B, Panigrahi BK. PNKLMF-based neural network control and learning-based HC MPPT technique for multiobjective grid integrated solar PV based distributed generating system. IEEE Trans Industr Inform 2019;15(6):3732–42.
[49] Kumar N, Singh B, Panigrahi BK. Framework of gradient descent least squares regression-based NN structure for power quality improvement in PV-integrated low-voltage weak grid system. IEEE Trans Ind Electron 2019;66(12):9724–33.
[50] Singh B, Kumar N, Panigrahi BK. "Steepest descent laplacian regression based neural network approach for optimal operation of grid supportive solar PV generation. IEEE Trans Circuits Syst II: Express Br 2021;68(6):1947–51.
[51] Nazir FU, Kumar N, Pal BC, Singh B, Panigrahi BK. Enhanced SOGI controller for weak grid integrated solar PV system. IEEE Trans Energy Convers 2020;35(3):1208–17.
[52] Kumar N, Singh B, Panigrahi BK. ANOVA Kernel Kalman Filter for multi-objective grid integrated solar photovoltaic-distribution static compensator *IEEE Trans CircuitsSyst I: Regul Pap* 2019;66(11):4256–64.
[53] Martin AD, Vazquez JR, Cano JM. MPPT in PV systems under partial shading conditions using artificial vision". Electr Power Syst Res 2018;162:89–98.
[54] Khan S, Alvi AN, Khan MZ, Awais Javed M, Alhazmi OH, Bouk SH. A novel superframe structure and optimal time slot allocation algorithm for IEEE 802.15.4–based Internet of things. Int J Distrib Sens Netw 2020;16(12).